RSC Advances

PAPER

View Article Online
View Journal | View Issue

Cite this: *RSC Adv.*, 2019, **9**, 10990

Targeting HER2-positive gastric cancer with a novel ^{18}F-labeled $Z_{HER2:342}$ probe

Yunyun Pan,†[a] Zhengyang Yang,†[a] Yuping Xu,[b] Zhicheng Bai,[b] Donghui Pan,[b] Runlin Yang,[b] Lizhen Wang,[b] Wenxian Guan*[a] and Min Yang*[b]

To realize the diagnosis of HER2-positive gastric cancer *via* PET imaging, herein, a new kind of ^{18}F-labeled HER2 affibody probe was created; the bifunctional maleimide derivative 1,4,7-triazacyclononane-1,4,7-triacetic acid (NOTA-MAL) was first coupled to a polypeptide, and the resulting compound was subsequently labeled with the ^{18}FAl complex. The binding characteristics of the probe were assessed using both *in vitro* studies and *in vivo* microPET imaging and biodistribution experiments. Immunohistochemical staining was performed to confirm the expression level of HER2 in the studied cell lines and tumors. The probe was successfully produced with the radiochemical purity of more than 95%. The NCI N87 cell-associated radioactivity was 19.31 ± 1.01% AD, and it decreased to 0.83 ± 0.04% AD per 10^6 cells after blocking HER2 as early as 15 minutes post-incubation ($p < 0.05$). A competition binding assay between radiolabeled and non-radioactive affibody molecules with NCI N87 indicated that the IC_{50} was 8.10 nM. The microPET imaging and biodistribution of human gastric cancer xenografts demonstrated that the probe could specifically accumulate in tumors at early time points. Protein detection confirmed a strong HER2 expression in NCIN87 and a weak HER2 expression in SGC7901. In conclusion, ^{18}FAl-NOTA-MAL-Cys-GGGRDN(M^0)-$Z_{HER2:342}$ was successfully prepared *via* a one-step method. The favorable preclinical data showed specific and effective tumor targeting capacity of the proposed probe; this revealed that the probe proposed herein might have potential application in gastric cancer imaging.

Received 14th December 2018
Accepted 17th March 2019

DOI: 10.1039/c8ra10271f

rsc.li/rsc-advances

1 Introduction

Gastric cancer, one of the most common malignancies, is the second highest contributor to cancer-related mortality in the world.[1] About 950 000 new cases of gastric cancer occurred in 2015 worldwide, and more than 70% of gastric cancer cases occurred in the developing countries, half of which occurred in Eastern Asia (primarily in China).[2] Currently, surgical operation may be the only method to realize a radical cure.[3] An accurate preoperative staging, especially that of the lymph node stage, of gastric cancer plays a vital role in determining an appropriate surgical method. Previous studies have focused on the role of ^{18}FDG-PET in the staging of gastric cancer.[4–7] The diagnostic effect of ^{18}FDG-PET on gastric cancer is still controversial[8] mainly due to the low sensitivity of ^{18}FDG-PET. The mechanism of action of ^{18}FDG-PET reflects active glucose metabolism associated with many kinds of tumors and may lead to limited sensitivity and specificity. The sensitivity and specificity of ^{18}FDG-PET in lymph node detection was 21–40% and 89–100%, respectively.[6] Consequently, to improve the diagnosis of gastric cancer by PET imaging, it is necessary to explore new kinds of agents targeting the biomarkers on primary or metastatic lesions.

Overexpression/amplification of HER2 occurs in diverse tumors and is correlated with cell proliferation and differentiation and initiation of cancer formation.[9] HER2 is a positive biomarker for the development and progression of gastric cancer. HER2 overexpression has been found in approximately 20–30% gastric cancer cases.[10–12] Currently, drugs, such as trastuzumab and lapatinib, targeting the HER2-positive gastric cancer are being extensively used as part of the treatment for patients with advanced gastric cancer as they seem to be more effective;[13,14] however, only few studies have been reported on gastric cancer-targeted diagnosis, especially with the HER2 protein as the target.

Affibody molecules are a novel class of polypeptides that originate from the scaffold Z domain derived from the B domain of the staphylococcal protein A.[15] Affibodies have shown many superiorities over antibodies and their derivatives. Due to their small size, the affibody molecules exhibit complementary capabilities to antibodies and a number of desired properties for targeted applications;[16] especially, size reduction leads to faster rate of blood clearance and improved tissue penetration;

[a]*Department of General Surgery, Drum Tower Hospital, Medical School of Nanjing University, 321 Zhongshan RD, Nanjing, China, 210008. E-mail: medguanwx@163.com*

[b]*Key Laboratory of Nuclear Medicine, Ministry of Health, Jiangsu Key Laboratory of Molecular Nuclear Medicine, Jiangsu Institute of Nuclear Medicine, Wuxi, Jiangsu, China, 214063. E-mail: yangmin@jsinm.org*

† These authors contribute equally in this work and share the first authorship.

moreover, affibody molecules have extraordinarily high affinity to targets, which is important for improving the targeting ability of drugs. All these features demonstrate that affibodies, including anti-HER2 binders, have the potential to function as ideal targeting carriers.

Herein, we aimed to accomplish the site-specific labelling of a novel $Z_{HER2:342}$ derivative and evaluate its targeting tracing capacity using HER2-expressing gastric cancer models.

2 Experimental

2.1. Labeling chemistry and quality control

2.1.1 General. Cys-GGGRDN(M^0)-$Z_{HER2:342}$ was kindly gifted by the Jiangsu Institute of Nuclear Medicine, and its chemical purity was greater than 95%. The maleimide derivative 1,4,7-triazacyclononane-1,4,7-triacetic acid (NOTA-MAL) was purchased from CheMatech (Dijon, France). ^{18}F was generated from a cyclotron through the proton irradiation of ^{18}O-enriched water (HM67, Sumitomo Heavy Industries). All other commercially obtained chemicals were of analytical grade and used without further purification. The Waters high-performance liquid chromatography (HPLC) system with the Waters 2998 photodiode array detector (PDA) and the preparative C18 HPLC column (5 μm, 250 × 19 mm, Waters 130Xbridge) was used to purify the precursor. Another Waters RP-HPLC system equipped with the Radiometric 610TR flow scintillation analyzer (Perkin Elmer), the Waters 2487 dual λ absorbance detector and the Luna C18 HPLC column (5 μm, 250 × 4.6 mm, Phenomenex) was used to analyze the radiolabeled compounds. The mobile phases A and B were 0.1% v/v trifluoroacetic acid in water and 0.1% v/v trifluoroacetic acid in acetonitrile, respectively.

2.1.2 Preparation of NOTA-MAL-Cys-M^0-$Z_{HER2:342}$. The precursor was obtained *via* the conjugation reaction of NOTA-MAL with Cys-M^0-$Z_{HER2:342}$ in the ammonium acetate–acetonitrile buffer (pH 7–8). The solutions were stirred overnight at 40 °C. The primary product was then injected into the preparative HPLC column; the gradient elution condition was as follows: the mobile phase changed from 95% A and 5% B (0–2 min) to 35% A and 65% B at 35 min at the flow rate of 5 mL min^{-1}. Then, the compounds were freeze-dried for storage.

2.1.3 Preparation of ^{18}FAl-NOTA-MAL-Cys-M^0-$Z_{HER2:342}$. A solution of NOTA-MAL-Cys-M^0-$Z_{HER2:342}$ (300 μg, 38 nmol) in sodium acetate buffer (20 μL, 0.2 M, pH 4) was added to a solution of aluminum chloride (6 μL, 2 mM in sodium acetate buffer, 0.5 M, pH 4) and $^{18}F^-$ (~3700 MBq) in 100 μL target water. After being heated at 100 °C for 10 min, the content of the vial was diluted with 10 mL water and loaded onto the activated Varian BOND ELUT C18 column. The column was washed with 10 mL PBS, and then, the desired content was eluted with 300 μL of 10 mM HCl in ethanol. The final product was reconstituted in saline and passed through a 0.22 μm Millipore filter into a sterile vial. The product was analyzed by analytical HPLC. The elution condition was the same as that in the case of preparative HPLC except that the flow rate was set at 1 mL min^{-1}. The scheme of the synthesis of the probe is shown in Fig. 1.

2.2. Cell culture and tumor model

The human gastric cancer cell lines NCI N87 (HER2-positive cell lines) and SGC 7901 (HER2-negative cell lines) were purchased from ATCC. Both cell lines were maintained in RPMI 1640 media (Gibco, USA) supplemented with 10% fetal bovine serum (Gibco, USA). The cells were cultured in a culture flask at 37 °C under a humidified atmosphere containing 5% CO_2.

All animal experiments were performed in accordance with the principles and procedures formulated by the National Animal Care and Use Committee. In addition, all animal experiments were approved by the Institutional Animal Care and Use Committee (IACUC) of Nanjing University. In the experiments with tumor-bearing mice, six- to eight-week-old female BALB/c nude mice were subcutaneously implanted with 1×10^7 of NCI N87 or 1×10^6 of SGC7901 cells on the shoulder. When the tumors grew to a diameter of about 4 mm, the mice were used for PET imaging and biodistribution experiments.

2.3. *In vitro* cell binding study

The *in vitro* cell uptake and blocking assays were performed to assess the binding characteristics of the probe. The suspension containing 1×10^6 cells was added to each of the γ count tubes on the day of labeling. A serum-free medium containing 1 μCi radiolabeled conjugates was added to the abovementioned tubes, and then, the solutions were gently mixed. The cells were incubated with the complex compounds at 37 °C for different time periods. At preplanned time points (*i.e.* 15, 30, 60, and 120 min after incubation), the corresponding tubes were centrifuged at 3000 rounds per minute for 5 min, and the cell pellets were formed. Then, the supernatant was completely removed, and the cell deposit was washed twice with PBS, followed by centrifugation. Moreover, the supernatant was discarded, and the radioactivity of the cell pellets in the tubes was measured using a γ counter (Perkin-Elmer, USA). For the blocking group, the HER2 proteins on NCI N87 were presaturated with an excess of non-labeled affibody 10 min before adding the labeled conjugates. The remaining steps were similar to those performed in the binding studies. The analysis was conducted in triplicate. The uptake results have been reported as the percentage of the added dose (%AD).

2.4. *In vitro* competition assay

The competition binding assay was conducted to study the affinity of the probe to HER2 with NCI N87. The cells were plated on a 96-well board at the cell density of 1×10^5 per aperture a day before conducting the experiments; after being washed twice with PBS, a binding buffer (serum-free medium), and a diluted competitor prepared herein (Cys-M^0-$Z_{HER2:342}$), the ^{18}F-labeled ligand was successively added to each cell dish to generate various concentration gradients of the competitor (from 0 to 2500 nM) and ensure the total volume of 200 μL. The board was placed at 37 °C for 1 hour. Thereafter, the supernatant liquid was removed, the wells were washed twice with ice-cold PBS, and the cells were then lysed with 0.1 M NaOH. The

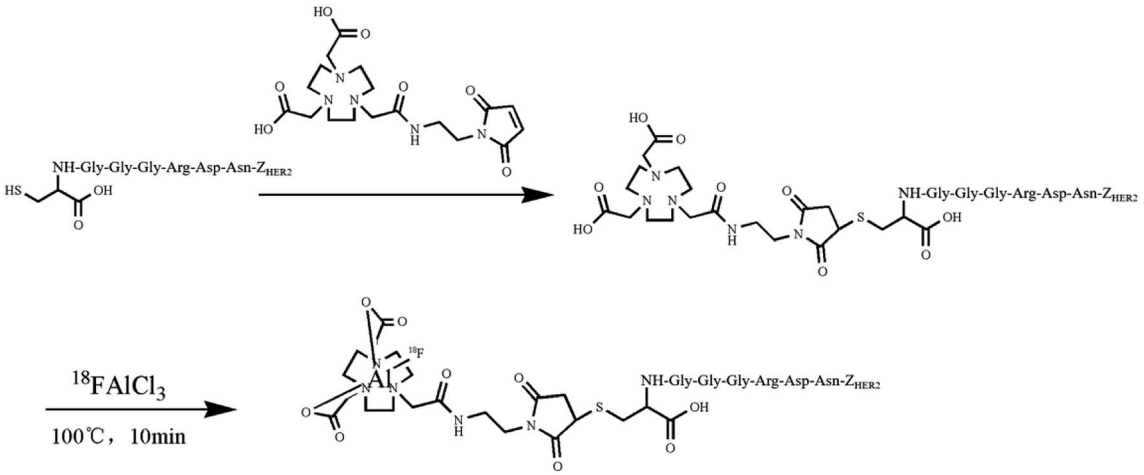

Fig. 1 The synthesis procedure of ^{18}F-NOTA-MAL-Cys-M^0-Z$_{HER2:342}$.

basic solutions were obtained, and the cells were washed with room-temperature PBS to completely acquire residual radioactivity; moreover, the cells were obtained and pooled with the corresponding alkaline solution in the γ counter tubes. Radioactivity was measured using the γ counter and analyzed *via* GraphPad Prism 5.0 (GraphPad Software, San Diego, USA). The IC_{50} value was calculated by the nonlinear regression model.

2.5. Immunohistochemical (IHC) staining

IHC staining was performed to investigate the levels of HER2 in cells and tumor tissues; the procedures of the IHC staining for both cells and tissues were conducted according to the manufacturer's instructions. For cell staining, the cells were plated on a 24-well board to an appropriate density in advance. For tissue staining, the fresh tumor tissues were fixed in a prepared fixation fluid. Sections were obtained by transferring the paraffin-embedded tissues onto a polylysine-coated slide with the thickness of 5 μm. The samples were co-incubated with the rabbit anti-HER2 antibody (GeneTech, China) for 2 hours at room temperature, followed by incubation with a goat anti-rabbit antibody (Vazyme Biotech, China) for 20 minutes.

2.6. Western blot

The cells were seeded in 60 mm dishes followed by incubation until the cells reached a confluence of 90%. The cells were then treated with lysis buffer on ice for 10 minutes, and cell lysates were obtained and centrifuged at 10 000–14 000 rcf at 4 °C for 5 min. The supernatant was stored at −20 °C until needed. The protein amount was measured using the BCA™ protein assay kit (Beyotime, China) and normalized using a bovine serum albumin concentration curve. The normalized samples with the same amount were subjected to sodium dodecyl sulfate (SDS)-polyacrylamide gel electrophoresis (PAGE) at 200 V for 35 min on a purchased gel (Invitrogen, USA) and then transferred to a polyvinylidene fluoride membrane (PVDF) at 150 mA for 90 min. The blots were blocked with 5% skim milk, dissolved in TBST for 1 h followed by washing three times with TBST, and then incubated overnight with a primary antibody (Abcam, UK) at 4 °C. After being washed again, the membranes were incubated with a secondary antibody (Abcam, UK) at room temperature for 2 h. Then, a western blot detection reagent was added to the membrane followed by visualization using the common film exposure method.

2.7. MicroPET imaging

Mice bearing tumors were injected with a diluted probe (3 MBq/200 μL/mouse) *via* the tail vein. The mice were anesthetized by isoflurane inhalation and placed in a prone position at the center of a scanner. Images were acquired at 0.5, 1, 2, and 4 h post injection for 10 minutes (three mice per group). The blocking groups were administered with blocking agents half an hour before the probe was injected. MicroPET imaging was performed using a microPET scanner (Siemens Medical Solutions, Germany). The regions of interest analysis for tumor and major organs was performed using the vendor software ASI Pro 6.7.1.1. The data was obtained from the max uptake level in the multiple ROI volume.

2.8. Biodistribution study

The animals were randomly assigned into different groups of three each. Animals were administered 1.3 MBq-radiolabeled conjugates in 100 μL normal saline, and the standard of the injected radioactive conjugates was simultaneously prepared. At predesignated time points, the mice were sacrificed. The main organs were obtained and weighed. The tissue uptake values were measured along with the standard using the γ counter and expressed as the percentage of the injected dose per gram of tissue (% ID g^{-1}).

2.9. Statistical analysis

Quantitative data were expressed as mean ± SD. Statistical analysis was performed using GraphPad Prism 5. The Student *T* test was used to compare the numerical data. $p < 0.05$ was considered statistically significant.

3 Results

3.1. Radiolabeling and quality control

The HPLC analysis of NOTA-MAL-Cys-M0-$Z_{HER2:342}$ indicated that the purity of the compound was more than 95% (Fig. 2a). The MS data confirmed that the relative molecular mass of this unlabeled intermediate was approximately 7790 (Fig. 2b). Furthermore, the HER2 targeting affibody was labeled with ^{18}F using the ^{18}FAl one-step method. The radiochemical purity of the product was more than 95% (Fig. 2c). The same retention

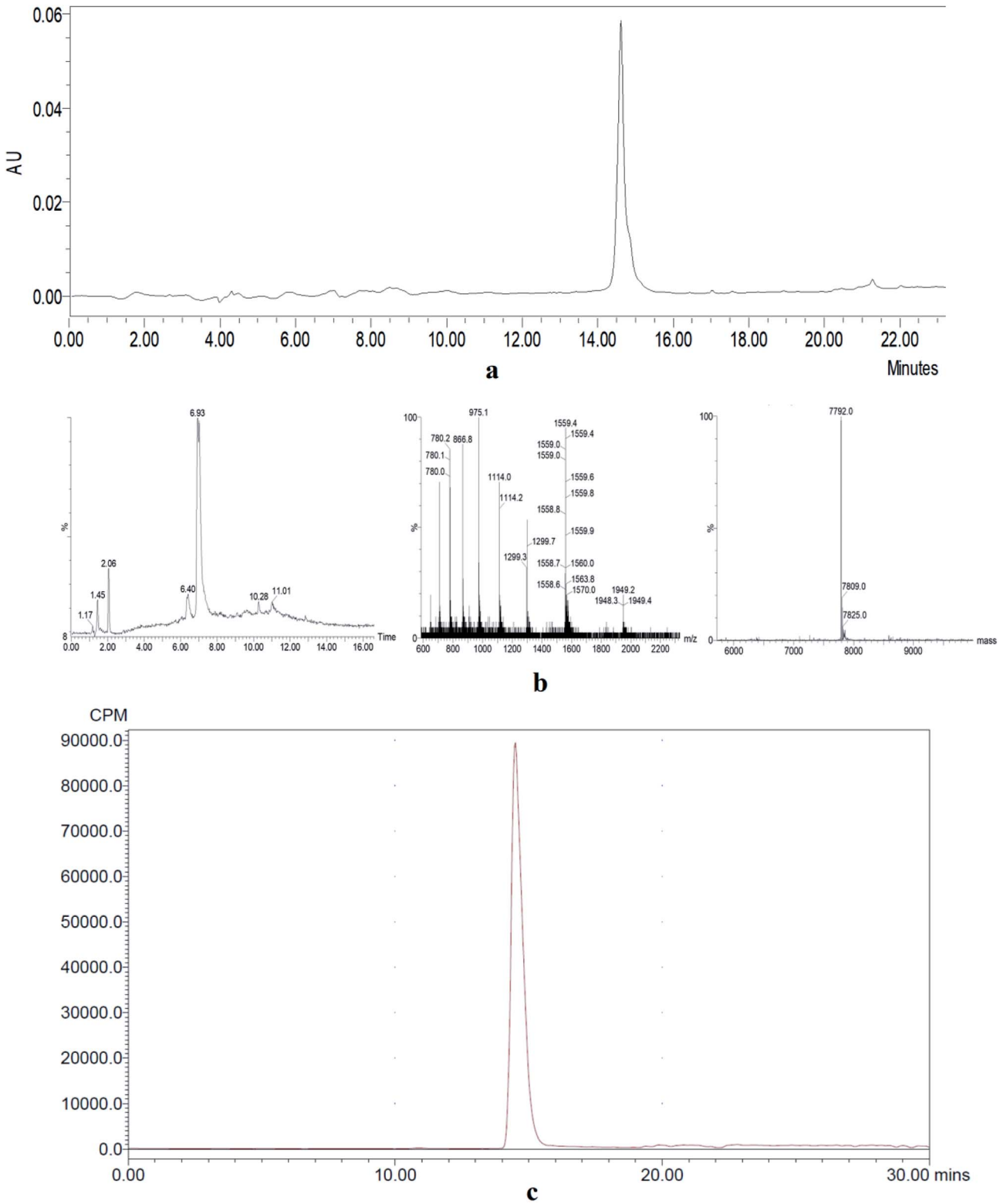

Fig. 2 (a) HPLC analysis of an unlabeled intermediate. (b) MS data of an unlabeled intermediate. (c) HPLC analysis of ^{18}FAl-NOTA-MAL-Cys-M^0-$Z_{HER2:342}$.

time (about 15 minutes) for the precursor and the labeled product preliminarily and basically indicated that the structure of the product was correct (Fig. 2a and c).

3.2. *In vitro* binding properties

The results of the *in vitro* cell-associated radioactivity as a function of time during the continuous incubation of gastric cancer cells with the ^{18}F labeled $Z_{HER2:342}$ at 37 °C are shown in Fig. 3a. The NCI N87 cell-associated radioactivity was close to the plateau (approximately 19.31 ± 1.01% ID/10^6 cells) as early as 15 minutes after incubation. Blocking analysis demonstrated that the binding of ^{18}F-$Z_{HER:342}$ to the living HER2 overexpressed cells was receptor-mediated since the cell binding level reduced from 19.31 ± 1.01% ID/10^6 cells to 0.83 ± 0.04% ID/10^6 cells ($p < 0.05$).

Competition binding assay with NCI N87 indicated that the probe could be displaced by unlabeled molecules of increasing concentration (Fig. 3b). The calculated IC_{50} of 8.10 nM demonstrated high binding affinity of Cys-M^0-$Z_{HER2:342}$ to HER2. This experiment also provided evidence for the receptor-mediated specific binding of Cys-M^0-$Z_{HER2:342}$ to HER2.

3.3. Protein detection

The IHC staining (both cells and tissues) and western blot were carried out to detect the HER2 protein expression. Both the NCI N87 cells and tumors were HER2 strong positive, and the HER2 proteins were mainly located on the membrane surface (dyed dark brown) (Fig. 4a and b); however, SGC7901 showed a weak HER2 expression level (Fig. 4c and d). Since the main function of IHC staining is localization, western blot has been performed for the semi quantitative assay of the cells. The mean density ratio of HER2 to actin for NCI N87 and SGC7901 was 1.03 and 0.43, respectively ($p < 0.05$) (Fig. 4e and f).

3.4. PET imaging and ROI analysis

The microPET imaging of nude mice bearing different human gastric cancer xenografts and the ROI qualitative analysis results are shown in Fig. 5. The NCI N87 tumors were shown clearly and intensively at all studied time points (Fig. 5a). The probe could quickly accumulate at the tumor site and nearly reached plateau with 14.05 ± 1.43% ID g^{-1} as soon as 30 min after injection. The uptake remained at the level of 14.34 ± 0.99% ID g^{-1} until 4 h post injection (Fig. 5d). After pre-saturating HER2 with cold compounds, the tumor uptake level decreased to 2.01 ± 0.08% ID g^{-1} at 1 h p.i. (Fig. 5b and e). This remarkable reduction ($p < 0.05$) was in agreement with the *in vitro* data. As expected, there was no obvious uptake in the control SGC 7901 xenografts (Fig. 5c). The weak absorption of 2.41 ± 0.23% ID g^{-1} was obtained at 1 h p.i. (Fig. 5e), which was comparable to that of the blocking group and suggested that the radioactivity concentration in SGC 7901 was mainly due to nonspecific accumulation. The liver and intestinal tract are not shown in the images. The bladder was the major non-targeting uptake organ; this indicated that the probe was mainly eliminated *via* the renal tract.

3.5. Biodistribution

Biodistribution studies were performed to further investigate the *in vivo* localization of ^{18}FAl-NOTA-MAL-Cys-M^0-$Z_{HER2:342}$. The results of the biodistribution studies are summarized in Table 1. The tumor accumulation of the tracer was 6.72 ± 1.94% ID g^{-1} at 30 min p.i. and remained at the high level of 7.37 ± 1.26% ID g^{-1} until 2 h p.i. The uptake values of liver were significantly lower than those of the tumors at all time points with the tumor-to-liver uptake value ratio of 5.35 ± 0.69 at 60 min p.i.; the tumor-to-blood uptake value ratio of 5.71 ± 0.14 at 30 min p.i. and 11.85 ± 1.93 at 2 h p.i. suggested a fast blood clearance rate. The radioactivity concentrations in all other normal organs except the kidney were very lower than those in the tumors. The kidney was the main non-specific uptake organ. Fig. 6a and b show the uptake values and tumors to normal tissue ratios. A two-week observation of mice was performed to evaluate the adverse effect of affibodies *in vivo*, and no adverse effects were observed after the injection. The diet and movement of the mice was as usual, and most of them died of cancer cachexia in about a month.

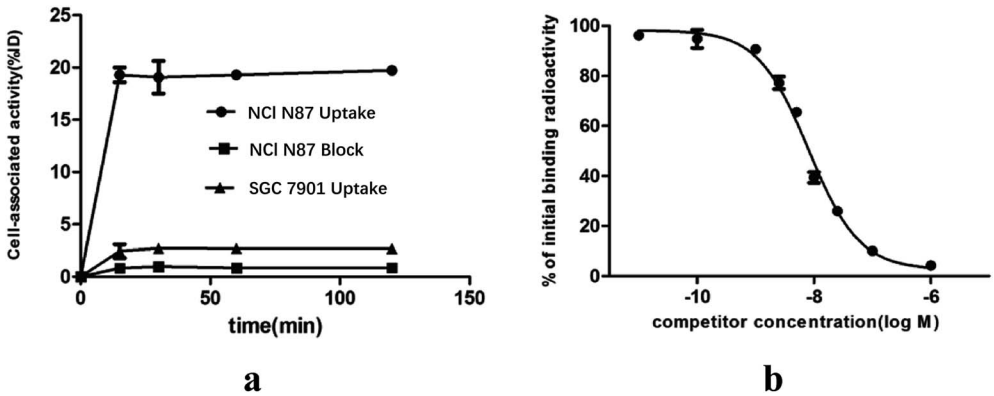

Fig. 3 (a) Cell uptake and blocking assay Cells with different HER2 expression levels were incubated with radiopharmaceuticals for 15, 30, 60, and 120 min. Cell-associated radioactivity was measured by the γ counter and presented as % AD. (b) Competition binding assay. The plots were described as the cell uptake percentage accounting for the initial binding radioactivity. The data are of competitor-free group ($n = 3$, mean ± SD).

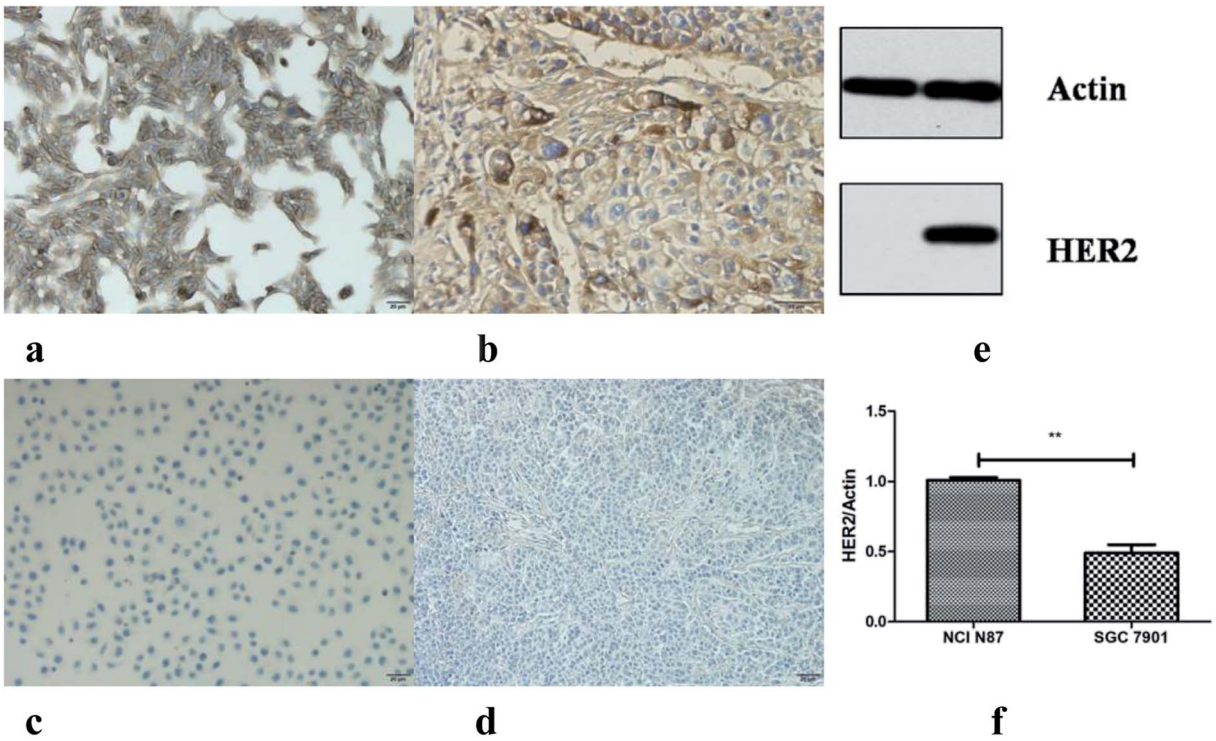

Fig. 4 HER2 test with IHC staining and western blot. NCI N87 cells and tumors ((a) ×200 fold; (b) ×400 fold) exhibited strong positive expression of HER2. HER2 proteins were mainly located on the cell membrane surface (dyed dark brown). SGC 7901 cells and tumors showed weak staining ((c) ×200 fold; (d) ×200 fold) when compared with the NCI N87 groups. The western blot results in (e) represent the actin and HER2 in SGC7901 (left) and NCI N87 (right). The mean density ratio of NCI N87 was significantly higher than that of SGC7901 ($p < 0.05$) (f).

4 Discussion

Tumor-targeted studies focusing on HER2 have been under active investigation and have made significant progress for a myriad of cancers. The Food and Drug Administration has approved that trastuzumab can be used to clinically treat patients with HER2-positive metastatic gastric cancer and gastroesophageal junction cancer.[17] HER2-targeted molecular therapies for gastric cancer have attracted extensive interest and become one of the research hotspots.[11,18] However, only few studies have been reported on the targeted diagnosis of gastric cancer. The available molecule for the diagnosis of gastric cancer *via* PET is primarily ^{18}FDG, which does not have strong targeting capacity. Therefore, to meet the requirements of targeted diagnosis and staging of gastric cancer, it is important to find a suitable and HER2-directed probe.

In the past few years, affibodies have attracted extensive interest because of their superiority over antibody-based tracers. A direct comparison between ^{124}I-labeled $Z_{HER2:342}$ and trastuzumab shows that the affibody molecules have superior properties mainly due to their small size. The tumor-to-normal organ ratios were remarkably higher for $Z_{HER2:342}$ even if the absolute tumor uptake was higher in the radiolabeled trastuzumab group of NCI N87 xenografts.[19] The sensitivity of imaging largely depends on the tumor to organ contrast.[20] A high tumor-to-normal organ ratio can improve the sensitivity of imaging due to the rapid clearance rate and strong tissue penetration ability of drugs towards normal tissues. Different kinds of affibodies have been radiolabeled with both single photon (^{99m}Tc[21] and ^{111}In[22]) and positron nuclides (^{68}Ga,[23,24] ^{64}Cu,[25] and ^{89}Zr[26]) for diagnostic applications. Compared to single-photon emission computed tomography (SPECT), PET provides better spatial and temporal resolution. ^{18}F is one of the most clinically used positron emitters with ideal nuclear physics properties (almost 100%, 0.64 MeV, $t_{1/2}$ = 109.5 min), which make it suitable for labeling small molecule polypeptides and PET imaging with better spatial resolutions.[20] A variety of methods have been used to label peptides with ^{18}F,[27–29] and the ^{18}FAl one-step method has shown attractive merits among them. Our teams have successfully accomplished ^{18}F radiolabeling of several vectors using this process.[30–32] Hence, we also chose this method to realize site-specific labelling by introducing a unique cysteine to the N-terminal of $Z_{HER2:342}$. Gly-Gly-Gly-Arg-Asp-Asn (GGGRDN) is a new kind of hydrophilic linker with favorable properties. Oligo-glycine can reduce the steric hindrance encountered during labeling. The positively charged Arg and negatively charged Asp form an ion pair that is beneficial for increasing hydrophilicity. The neutral Asn also acts as a hydrophilic spacer. Our previous studies have proved that the modified ATBBN peptides (^{18}F-FP-MATBBN,^{68}Ga-NOTA-MATBBN) have enhanced hydrophilicity, and better contrast imaging with clear lower abdominal background could be acquired when compared with the case of respective unmodified peptides (^{18}F-FP-ATBBN,^{68}Ga-NOTA-ATBBN).[33,34] Decreased liver and intestine non-specific accumulation was critical for mapping the abdominal primary and

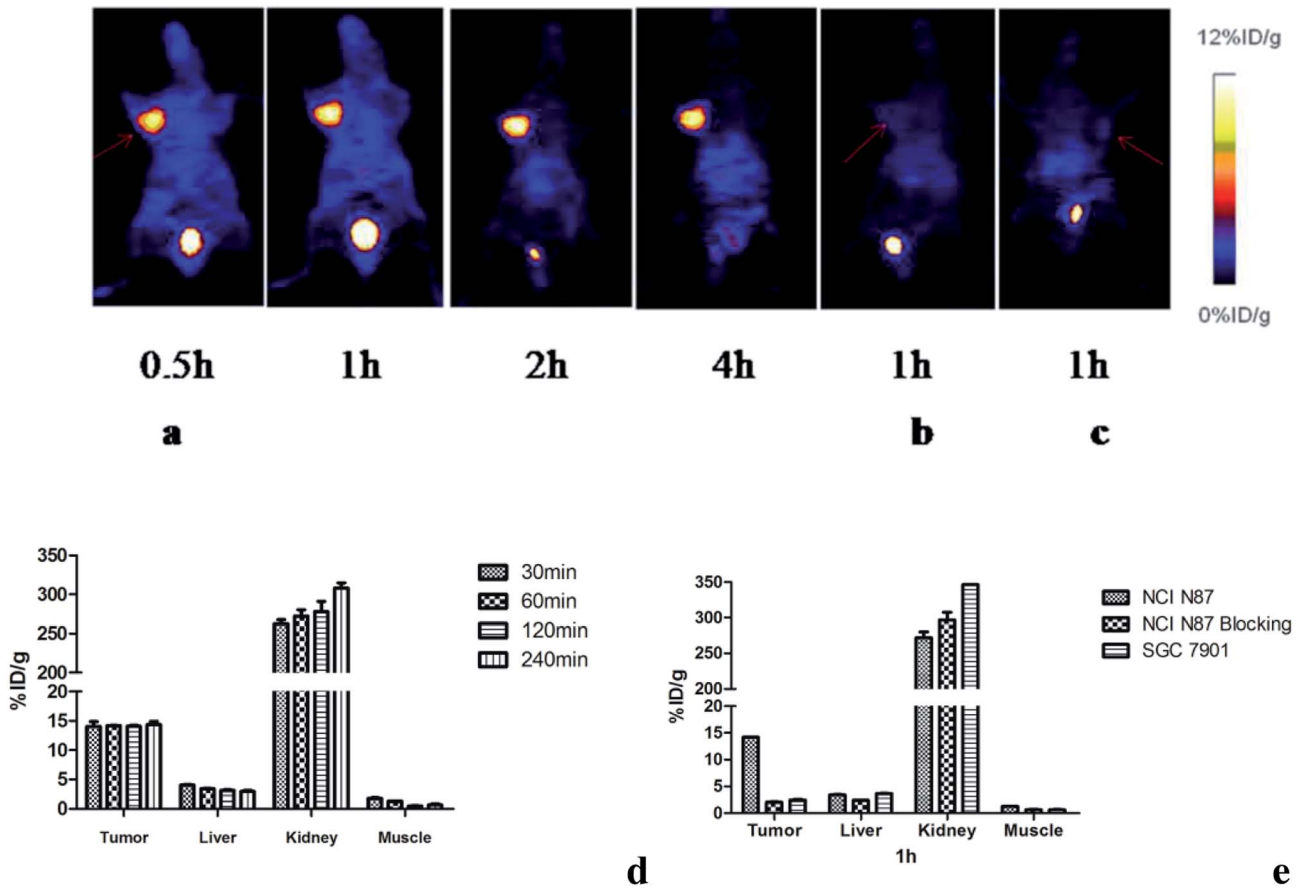

Fig. 5 MicroPET imaging and ROI analysis. The images of NCI N87 (0.5 h, 1 h, 2 h, and 4 h p.i.) (a) and SGC7901 (1 h p.i.) models (c) acquired at different time points after administration. Blocking images of the NCI N87 models were also obtained at 1 h p.i. (b). The ROI analysis results are shown in (d) and (e). The uptake data were described as % ID g^{-1} ($n = 3$, mean ± SD).

secondary lesions. Based on the previously reported promising results, we intended to improve the $Z_{HER2:342}$-based radiotracers by inserting an M^0 linker at the N-terminal. Therefore, we established a novel kind of HER2-targeted probe (^{18}FAl-NOTA-MAL-Cys-M^0-$Z_{HER2:342}$) that functioned as an imaging agent, and it was used to target gastric cancer for the first time.

The probe showed inspiring HER2 binding affinity and specificity. Its affinity in the low nanomolar range was comparable to that of another kind of anti-HER2 affibody, ^{18}F-NOTA-$Z_{HER2:2395}$, towards the SKOV3 cells (8.1 nM *versus* 5.0 nM, respectively).[35] The appreciably lower cell-associated radioactivity for SGC 7901 reflected the lower expression level of HER2, which was consistent with the protein detection results and comparable to that observed in the blocking group; this further confirmed the binding specificity of the probe. HER2-positive NCI N87 tumors could be clearly visualized at early time points and were clearly observed until 4 h p.i. *via* microPET imaging. However, the SGC7901 tumors only displayed rough sketches. These imaging results revealed that the probe could quickly accumulate in the HER2 overexpressing tumors and had strong targeted retention ability. The tissue uptake data obtained *via* the biodistribution studies were overall lower than those obtained *via* the microPET imaging. The possible reason was that in the imaging studies, the radioactivity was obtained from the max pixel values within the multiple ROI volume, whereas in the biodistribution studies, it was obtained from the mean uptake concentration, which considered all parts of the organ. Overall, the biodistribution results corresponded well with the microPET imaging results and exhibited favorable tumor targeting capability of radiopharmaceuticals. The T/B ratios were similar to that of ^{18}F-FBEM-$Z_{HER2:342}$ observed in the SKOV3 models at 1 h p.i. ((9.74 ± 0.77)% ID g^{-1} *versus* (7.5 ± 4.5)% ID g^{-1}); however they were lower at 2 h p.i. ((12.7 ± 1.73)% ID g^{-1} *versus* (23 ± 5.5)% ID g^{-1}). This indicated that the

Table 1 Biodistribution results for ^{18}FAl-NOTA-MAL-Cys-M^0-$Z_{HER2:342}$ in NCI N87 xenograft models ($n = 3$ per group)

Organs (% ID g^{-1})	30 min	60 min	120 min
Blood	1.32 ± 0.38	0.75 ± 0.17	0.72 ± 0.21
Brain	0.11 ± 0.06	0.06 ± 0.01	0.06 ± 0.01
Liver	1.58 ± 0.50	1.37 ± 0.34	1.89 ± 0.06
Spleen	0.70 ± 0.34	0.55 ± 0.09	0.84 ± 0.18
Kidney	238.75 ± 2.0	310.56 ± 44.51	379.80 ± 16.42
Stomach	0.59 ± 0.15	0.36 ± 0.17	0.29 ± 0.25
Intestine	1.07 ± 0.11	1.07 ± 0.06	1.01 ± 0.23
Muscle	1.05 ± 0.78	0.38 ± 0.11	0.61 ± 0.17
Pancreas	0.53 ± 0.13	0.34 ± 0.06	0.29 ± 0.03
Fat	0.81 ± 0.34	0.61 ± 0.26	0.89 ± 0.35
Bone	1.73 ± 0.51	1.42 ± 0.59	1.54 ± 0.53
Tumor	6.72 ± 1.94	7.00 ± 1.42	7.37 ± 1.26

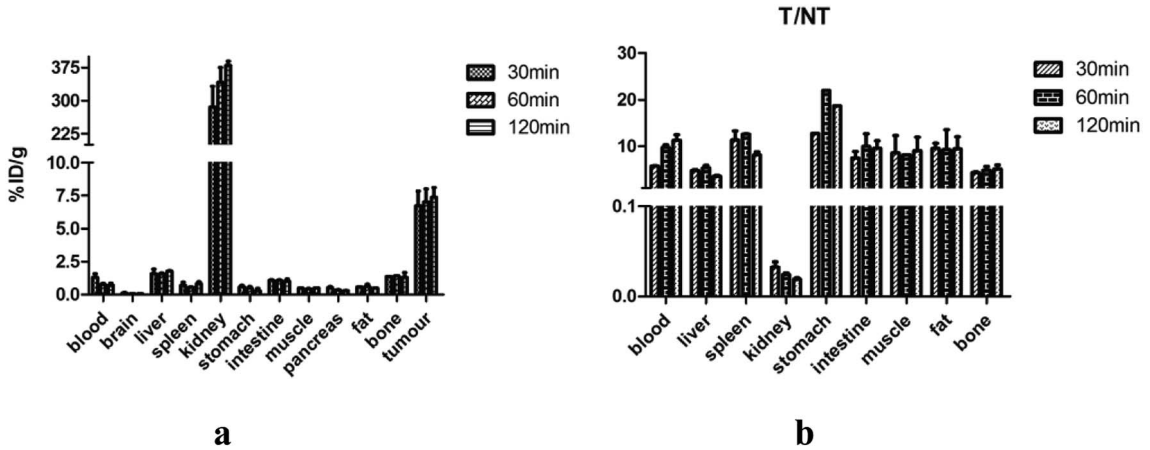

Fig. 6 *In vivo* biodistribution. Biodistribution of the probe in NCI N87 models at different time points after injection (a). Tumor-to-normal tissue ratios of main organs (b). Data are presented as an average ± SD from three animals per group (n = 3, mean ± SD).

clearance rate of ^{18}FAl-NOTA-MAL-cys-M^0-Z$_{HER2:342}$ from circulation was relatively slower than that of FBEM-Z$_{HER2:342}$ in the first two hours. However, the images obtained were of high contrast despite the relatively slower blood clearance. It could be concluded that the tumor-to-organ ratios would further increase over time, as reported in other previous studies.[19,36] Thus, biodistribution for a longer time may be necessary to further assay the *in vivo* properties of the probe. The radioactivities in the liver were under 2% ID g^{-1} at all the studied time points. The excretion of the probe predominantly occurred *via* the urinary tract with the highest accumulation of the probe among all the nontargeted organs due to the small size of the probe and the introduction of a hydrophilic group. Another possible explanation was that radiolabeling using the ^{18}FAl method was residualizing; this was similar to the case of radiometal labels with long-term retention in the renal tract.

Overall, the ^{18}F-labeled Z$_{HER2:342}$ modified with GGGRDN is a promising probe to target gastric cancer with high contrast and may improve the diagnosis and staging of gastric cancer. It is necessary to further evaluate its features by directly comparing it with ^{18}F-labeled Z$_{HER2:342}$ without modification under the same conditions.

5 Conclusion

Herein, hydrophilic GGGRDN-modified Z$_{HER2:342}$ was successfully conjugated to NOTA-MAL and conveniently tagged with ^{18}F using the ^{18}FAl one-step method. The obtained 18FAl-NOTA-MAL-Cys-GGGRDN-Z$_{HER2:342}$ could trace gastric cancer with high specificity, affinity and tumor-targeting property. ^{18}FAl-NOTA-MAL-cys-GGGRDN-Z$_{HER2:342}$ is a promising tumor-targeted tool that may improve the diagnosis of HER2-positive gastric cancer.

Author contributions

Wenxian Guan and Min Yang designed the research; Zhengyang Yang and Yuping Xu collected the data; Zhicheng Bai, Donghui Pan, Runlin Yang and Lizhen Wang performed data analysis; Yunyun Pan wrote the manuscript; Wenxian Guan and Min Yang reviewed the manuscript.

Conflicts of interest

None.

Abbreviation

HER2	Human epidermal growth factor receptor-2
PET	Positron emission tomography
^{18}FDG	^{18}F-deoxyglucose
HPLC	High-performance liquid chromatography
MS	Mass spectrometry
PDA	Photodiode array detector
PBS	Phosphate-buffered saline
IHC	Immunohistochemical
ROI	Region of interest
SD	Standard deviation
SPECT	Single-photon emission computed tomography
GGGRDN	Gly-Gly-Gly-Arg-Asp-Asn

Acknowledgements

This work was supported by the National Natural Science Foundation of China (81372364 and 81472749) and Ministry of Science and Technology of the People's Republic of China (2016YFC0104105).

References

1 E. V. Cutsem, X. Sagaert, B. Topal, K. Haustermans and H. Prenen, *Lancet*, 2016, **388**, 2654–2664.
2 A. Shichao, Z. Shuang, L. Zhijian, S. Feng, H. Xingchen, C. Feng, G. Wenxian and W. Jianquan, *RSC Adv.*, 2018, **8**, 30012–30020.
3 H. Zhang, H. Liu, Z. Shen, C. Lin, X. Wang, J. Qin, X. Qin, J. Xu and Y. Sun, *Ann. Surg.*, 2018, **267**, 311–318.

4 H. Zou and Y. Zhao, *Surgical Oncology*, 2013, **22**, 162–166.
5 N. Bulut and B. Yılmaz, *Int. J. STD AIDS*, 2018, **29**, 96–98.
6 H. Shimada, S. Okazumi, M. Koyama and K. Murakami, *Gastric Cancer*, 2011, **14**, 13–21.
7 E. Y. Kim, W. J. Lee, D. Choi, S. J. Lee, J. Y. Choi, B. T. Kim and H. S. Kim, *Eur. J. Radiol.*, 2011, **79**, 183–188.
8 C. Altini, A. N. Asabella, A. D. Palo, M. Fanelli, C. Ferrari, M. Moschetta and G. Rubini, *Medicine*, 2015, **94**, e864.
9 N. V. Jordan, A. Bardia, B. S. Wittner, C. Benes, M. Ligorio, Y. Zheng, M. Yu, T. K. Sundaresan, J. A. Licausi, R. Desai, R. M. O'Keefe, R. Y. Ebright, M. Boukhali, S. Sil, M. L. Onozato, A. J. Iafrate, R. Kapur, D. Sgroi, D. T. Ting, M. Toner, S. Ramaswamy, W. Haas, S. Maheswaran and D. A. Haber, *Nature*, 2016, **537**, 102–106.
10 S. Yun, J. Koh, S. K. Nam, J. O. Park, S. M. Lee, K. Lee, K. S. Lee, S. H. Ahn, D. J. Park, H. H. Kim, G. Choe, W. H. Kim and H. S. Lee, *Gastric Cancer*, 2018, **21**, 225–236.
11 E. V. Cutsem, Y. J. Bang, Y. F. Feng, J. M. Xu, K. W. Lee, S. C. Jiao, J. L. Chong, R. I. López-Sanchez, T. Price, O. Gladkov, O. Stoss, J. Hill, V. Ng, M. Lehle, M. Thomas, A. Kiermaier and J. Rüschoff, *Gastric Cancer*, 2015, **18**, 476–484.
12 O. Gumusay, M. Benekli, O. Ekinci, M. Baykara, A. Ozet, U. Coskun, U. Demirci, A. Uner, A. Dursun, E. Y. Atak and S. Buyukberber, *Jpn. J. Clin. Oncol.*, 2015, **45**, 416–421.
13 J. H. Yi, J. H. Kang, I. G. Hwang, H. K. Ahn, H. J. Baek, S. I. Lee, D. H. Lim, Y. W. Won, J. H. Ji, H. S. Kim, S. Y. Rha, S. Y. Oh, K. E. Lee, T. Lim, C. H. Maeng, M. J. Kim, S. T. Kim, J. Lee, J. O. Park, Y. S. Park, H. Y. Lim, W. K. Kang and D. H. Park, *Cancer Res. Treat.*, 2016, **48**, 553–560.
14 T. Matsuoka and M. Yashiro, *World J. Clin. Cases*, 2015, **3**, 42–51.
15 S. Ståhl, T. Gräslund, A. E. Karlström, F. Y. Frejd, P. A. Nygren and J. Löfblom, *Trends Biotechnol.*, 2017, **35**, 691–712.
16 H. Shi, R. Yan, L. Wu, Y. Sun, S. Liu, Z. Zhou, J. He and d. Ye, *Acta Biomater.*, 2018, **72**, 256–265.
17 S. Han, Y. Meng, Q. Tong, G. Li, X. Zhang, Y. Chen, S. Hu, L. Zheng, W. Tan, H. Li, Y. Chen, G. Zhang, B. Li and Y. Guo, *mAbs*, 2014, **6**, 403–408.
18 K. Ito, M. Mitsunaga, S. Arihiro, M. Saruta, M. Matsuoka, H. Kobayashi and H. Tajiri, *BMC Cancer*, 2016, **16**, 37.
19 A. Orlova, H. Wållberg, S. S. Elander and V. Tolmachev, *J. Nucl. Med.*, 2009, **50**, 417–425.
20 D. Rosik, A. Thibblin, G. Antoni, H. Honarvar, J. Strand, R. K. Selvaraju, M. Altai, A. Orlova, A. E. Karlström and V. Tolmachev, *Bioconjugate Chem.*, 2014, **25**, 82–92.
21 V. Tolmachev, C. Hofström, J. Malmberg, S. Ahlgren, S. J. Hosseinimehr, M. Sandström, L. Abrahmsén, A. Orlova and T. Gräslund, *Bioconjugate Chem.*, 2010, **21**, 2013–2022.
22 M. Altai, J. Strand, D. Rosik, R. K. Selvaraju, A. E. Karlström, A. Orlova and V. Tolmachev, *Bioconjugate Chem.*, 2013, **24**, 1102–1109.
23 J. Strand, Z. Varasteh, O. Eriksson, L. Abrahmsen, A. Orlova and V. Tolmachev, *Mol. Pharm.*, 2014, **11**, 3957–3964.
24 J. Sörensen, I. Velikyan, D. Sandberg, A. Wennborg, J. Feldwisch, V. Tolmachev, A. Orlova, M. Sandström, M. Lubberink, H. Olofsson, J. Carlsson and H. Lindman, *Theranostics*, 2016, **6**, 262–271.
25 M. A. Kruziki, B. A. Case, J. Y. Chan, E. J. Zudock, D. R. Woldring, D. Yee and B. J. Hackel, *Mol. Pharm.*, 2016, **13**, 3747–3755.
26 J. Garousi, K. G. Andersson, B. Mitran, M. L. Pichl, S. Ståhl, A. Orlova, J. Löfblom and V. Tolmachev, *Int. J. Oncol.*, 2016, **48**, 1325–1332.
27 S. Verhoog, C. W. Kee, Y. Wang, T. Khotavivattana, T. C. Wilson, V. Kersemans, S. Smart, M. Tredwell, B. G. Davis and V. Gouverneur, *J. Am. Chem. Soc.*, 2018, **140**, 1572–1575.
28 N. Okamura, S. Furumoto, M. T. F. Tavoletti, R. S. Mulligan, R. Harada, P. Yates, S. Pejoska, Y. Kudo, C. L. Masters, K. Yanai, C. C. Rowe and V. L. Villemagne, *Brain*, 2014, **137**, 1762–1771.
29 E. Panagiotidis, A. Alshammari, S. Michopoulou, E. Skoura, K. Naik, E. Maragkoudakis, M. Mohmaduvesh, M. A. Harbi, M. Belda, M. E. Caplin, C. Toumpanakis and J. Bomanji, *J. Nucl. Med.*, 2017, **58**, 91–96.
30 C. Zhu, Q. Xu, D. Pan, Y. Xu, P. Liu, R. Yang, L. Wang, X. Sun, S. Luo and M. Yang, *Contrast Media Mol. Imaging*, 2016, **11**, 99–105.
31 Q. Xu, C. Zhu, Y. Xu, D. Pan, P. Liu, R. Yang, L. Wang, F. Chen, X. Sun, S. Luo and M. Yang, *J. Drug Targeting*, 2015, **23**, 813–820.
32 Y. Xu, D. Pan, C. Zhu, Q. Xu, L. Wang, F. Chen, R. Yang, S. Luo, M. Yang and Y. Yan, *Mol. Imaging Biol.*, 2014, **16**, 578–585.
33 M. Yang, H. Gao, Y. Zhou, Y. Ma, Q. Quan, L. Lang, K. Chen, G. Niu, Y. Yan and X. Chen, *Theranostics*, 2011, **1**, 220–229.
34 D. Pan, Y. P. Xu, R. H. Yang, L. Wang, F. Chen, S. Luo, M. Yang and Y. Yan, *Amino Acids*, 2014, **46**, 1481–1489.
35 S. Heskamp, P. Laverman, D. Rosik, F. Boschetti, W. T. V. Graaf, W. J. Oyen, H. W. V. Laarhoven, V. Tolmachev and O. C. Boerman, *J. Nucl. Med.*, 2012, **53**, 146–153.
36 G. K. Marek, D. O. Kiesewetter, L. Martiniova, E. Jagoda, S. B. Lee and J. Capala, *Eur. J. Nucl. Med. Mol. Imaging*, 2008, **35**, 1008–1018.